Tensor-Based Near-Field Localization in Bistatic MIMO Radar Systems

Ivan Podkurkov[1,2], Liana Hamidullina[1,2], Evgenii Traikov[1,2], Martin Haardt[1] and Adel Nadeev[2]
[1]Communication Research Laboratory, Ilmenau University of Technology, Ilmenau, Germany
[2]German-Russian Institute of Advanced Technologies, Kazan National Research Technical University, Kazan, Russia
ivan.podkurkov@tu-ilmenau.de, Martin.Haardt@tu-ilmenau.de

***Abstract*—Several new algorithms have been proposed recently for near-field target localization and parameter estimation in Bistatic MIMO Radar systems. The new approaches include the usage of the exact spherical wavefront model, which avoids a systematic error introduced by the Fresnel approximation that is commonly made on impinging wavefronts in order to simplify the estimation problem. In this paper, we propose a new Tensor-based Near-Field Localization (TeNFiL) algorithm that utilizes the Canonical Polyadic (CP) decomposition of the received data in order to obtain high-resolution estimates of the parameters of the dominant targets that are automatically paired. Those parameters include the distances to the transmit and the receive reference antennas, the directions of departure (DoDs) and the directions of arrival (DoAs). TeNFiL is extended to the estimation in three-dimensional space and is applicable to arbitrary antenna array geometries. We develop a new reliability test and a new reliability measure for TeNFiL. The TeNFiL algorithm is based on the Semi-algebraic framework for approximate CP decompositions via Simultaneous Matrix Diagonalizations (SECSI). It is used to compute an approximate low rank CP decomposition of the noise corrupted measurements in a robust and efficient way. The simulations show that TeNFiL outperforms recent state of the art algorithms, especially if the targets are closely spaced.**

***Index Terms*—Near Field, Spherical Wavefront, SECSI, CPD, TeNFiL, Bistatic, MIMO Radar**

I. Introduction

The concept of MIMO Radar is a new technology that has attracted a lot of research attention recently [6], [13]. The new concept of MIMO Radar allows to reduce the number of antennas required for radar estimation by creating virtual arrays with an increased number of virtual elements that, in turn, provides multiple diversities in the spatial domain. Those diversities allow an improved estimation of the target parameters with less hardware requirements.

Most of the research in this area uses the far-field assumption, which implies that the shape of the incoming wavefront is assumed to be planar. Although this assumption greatly simplifies the estimation problem, it does not cover all practical usage scenarios, especially for cases when the targets are located much closer to the transmit and/or receive arrays. In the near-field problem, the spherical shapes of the wavefronts emitted by the transmit antennas and reflected by the targets should be considered. Although this complicates the estimation problem on the one hand, on the other, it provides means to estimate the range parameters since in this case the array manifold depends on the DoDs/AoAs as well as the distance to the target.

The common approximation for the spherical wavefronts used in literature on near-field localization is the Fresnel approximation [10], [16]–[18], which approximates a spherical wavefront using the second order Taylor expansion of the true phase distribution of the wavefront across the antennas. The recently proposed subspace based algorithm in [4] avoids the use of the Fresnel approximation and relies on the exact spherical model of the impinging wavefronts. It is based on the Eigenvalue Decompositions (EVD) of matrices computed from a low rank approximations of the sub-blocks of the sample covariance matrix. The Cramér Rao Bound (CRB) for near-field localization in two-dimensional (2-D) space was analyzed in [1], [12], and particularly for exact wavefront model in [2]. Then, the derived CRB was used to analyze and optimize a linear antenna array geometry in 2-D space in [7]. The use of the exact spherical wavefront model improves the estimation accuracy of the model in realistic scenarios and avoids systematic errors introduced by the Fresnel approximation.

In this paper we propose the Tensor-based Near-Field Localization algorithm (TeNFiL) based on the exact spherical wavefront model presented in [4] for the 2-D space. The signal model allows us to arrange the data in the form of the tensor with a low rank structure. Taking an approximate CP decomposition of the noise corrupted data we can estimate the factor matrices of the low rank representation. Those factor matrices represent array steering matrices of the transmit and the receive array, that then can be used to solve a similar system of equations, which was also defined in [4] for a special case of uniform linear array (ULA) in 2-D space. A tensor-based model for near-field localization has already been briefly discussed in [16], where the parameters were obtained from array steering matrices using an iterative solution of an optimization problem with a cost function defined in the least squares sense with respect to the elements of the array steering matrices. In contrast, the TeNFiL algorithm provides a closed form solution to the estimation problem in three-dimensional (3-D) space that is in general applicable to arbitrary array geometries. Moreover, [16] relies on the Alternating Least Squares (ALS) based COMFAC algorithm proposed in [3], while we use the SECSI framework that has an improved performance, especially in critical scenarios (closely spaced targets), which is shown in [14] and [15]. Furthermore, TeNFiL includes a new reliability test and a new reliability measure.

ISBN 978-3-8007-4541-8

Notation: Upper-case and lower-case bold-faced letters denote matrices and vectors, respectively. Upper-case Greek letter denote sets and bold faced calligraphic letters denote tensors. The elements of vectors are denoted as follows: $(\boldsymbol{a})_{(i)}$ denotes i-th element of a vector $\boldsymbol{a}$. The r-mode vectors of a tensor are obtained by varying the r-th index of the tensor while keeping all other indices fixed. The r-mode unfolding of the tensor $\boldsymbol{\mathcal{X}}$ is obtained by stacking its r-mode vectors into a matrix in reverse-cyclical order [5], denoted as $[\boldsymbol{\mathcal{X}}]_{(r)}$. The r-mode product between a tensor $\boldsymbol{\mathcal{X}}$ and a matrix $\boldsymbol{A}$ is denoted as $\boldsymbol{\mathcal{X}} \times_r \boldsymbol{A}$ [5], and the Khatri-Rao product between matrices $\boldsymbol{A}$ and $\boldsymbol{B}$ is denoted as $\boldsymbol{A} \diamond \boldsymbol{B}$. The conjugate, transpose and Hermitian transpose are denoted by $\{\cdot\}^*$, $\{\cdot\}^T$, and $\{\cdot\}^{\mathrm{H}}$, respectively. To ease the notation, in the following we assume that symbols x, y and z will always refer to Cartesian coordinates of the targets or antennas. Furthermore, the symbols ρ, ϕ, and θ will always denote the distance, azimuth and elevation of the targets, respectively.

II. System model

We consider a Bistatic MIMO Radar that consists of transmit and receive antenna arrays. Each antenna in the MIMO Radar system transmits signals that are orthogonal to each other. Those signals are then matched-filtered at each antenna of the receive array using the transmitted waveforms that are assumed to be known at the receiver. Thus, the superimposed reflected wavefronts created by the signals transmitted from different antennas can be well separated at the receiver, providing a virtual array with an increased number of elements.

In this paper we consider parameter estimation in both 2-D and 3-D spaces. In the 2-D case, the estimated parameters are the range and azimuth angle of the dominant radar targets. In the 3-D case, we additionally estimate the elevation angle for each target. The considered system model and proposed algorithm are applicable to arrays of arbitrary geometries, provided that those are known, but we will consider uniform linear array (ULA) for the 2-D case and uniform rectangular array (URA) for the 3-D case as special cases. It can also be shown that if the arrays exhibit diversity in all space directions (i.e., the antenna array does not lie in a lower-dimensional subspace), it is possible to estimate the locations of the targets in the complete 2-D space or the complete 3-D space, respectively.

A. Scenario

Let M_T denote the number of antennas in the transmit array, and M_R denote the number of antennas in the receive array. The number of targets present is denoted by H, and some of them are assumed to be in the near-field zone of both arrays (in general, some of them can also be in the far-field), i.e., they are close enough to the transmitter and receiver such that the wavefronts of the impinging and reflecting waves can be considered as spherical.

In the 3-D space, the locations of transmit/receive antennas are defined using Cartesian coordinates with respect to the reference transmit/receive antenna, i.e., it is assumed that the reference antennas are located at the origin. From now on, we will refer to the respective systems of coordinates as "local transmit" and "local receive" systems of coordinates. The m-th transmit antenna location is described by its Cartesian coordinates $\{x_{T,m}, y_{T,m}, z_{T,m}\}$, $\forall m \in \{1, ..., M_T\}$, and same as the n-th receive antenna location is described by $\{x_{R,n}, y_{R,n}, z_{R,n}\}$, $\forall n \in \{1, ..., M_R\}$. Since the reference antennas are always at the origin, then $x_{T,1} = y_{T,1} = z_{T,1} = x_{R,1} = y_{R,1} = z_{R,1} = 0$. In 2-D space we assume that $z_{T,m} = z_{R,n} = 0$ $\forall m, n$.

Since we are considering a Bistatic scenario, the receive reference antenna has coordinates $\{x_R, y_R, z_R\}$ with respect to the transmit reference antenna. In 2-D space we assume $z_R = 0$.

Each target in 3-D space is characterized by a set of six parameters $\boldsymbol{\Theta}_h^{(s)} = \{\rho_{T,h}, \phi_{T,h}, \theta_{T,h}, \rho_{R,h}, \phi_{R,h}, \theta_{R,h}\}$, $\forall h \in \{1, ..., H\}$, where $\rho_{T,h}$ and $\rho_{R,h}$ are the distances from the h-th target to the reference transmit and receive antennas, respectively, $\phi_{T,h}$, $\phi_{R,h}$ are the azimuths and $\theta_{T,h}$, $\theta_{R,h}$ are the elevation angles, defined with respect to the local transmit and

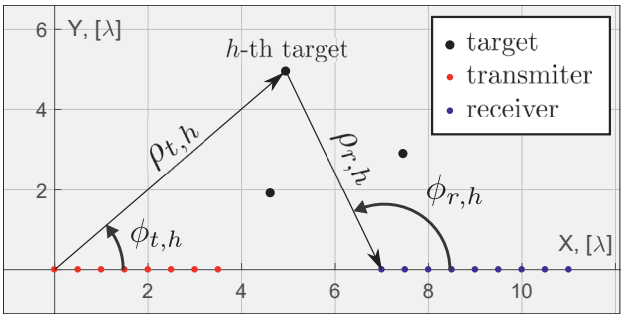

Fig. 1. 2-D system scenario. The transmit and receive array are depicted using red and blue dots, respectively. The first antennas of the arrays are chosen as reference antennas. The black dots denote radar targets. The figure also shows the four parameters of one of the targets.

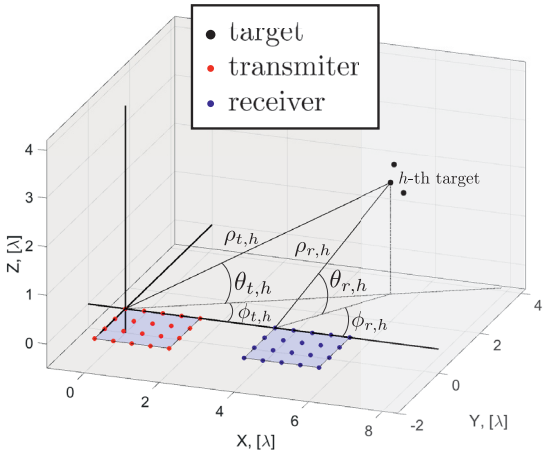

Fig. 2. 3-D system scenario. The transmit and receive array are depicted using red and blue dots, respectively. The first antennas of the arrays are chosen as reference antennas. The black dots denote radar targets. The figure also shows the six parameters of one of the targets.

ISBN 978-3-8007-4541-8

$$\delta^t_{m,h} = \sqrt{(x_{T,h} - x_{T,m})^2 + (y_{T,h} - y_{T,m})^2 + (z_{T,h} - z_{T,m})^2} - \rho_{T,h} \quad \forall m, h \tag{1}$$

$$\delta^r_{n,h} = \sqrt{(x_{R,h} - x_{R,n})^2 + (y_{R,h} - y_{R,n})^2 + (z_{R,h} - z_{R,n})^2} - \rho_{R,h} \quad \forall n, h \tag{2}$$

the local receive systems of coordinates. For notational convenience, we also introduce a set of Cartesian coordinates of the h-th target as $\boldsymbol{\Theta}^{(c)}_h = \{x_{T,h}, y_{T,h}, z_{T,h}, x_{R,h}, y_{R,h}, z_{R,h}\}$, $\forall h \in \{1, ..., H\}$.

In the 2-D space, the parameter sets for each target are reduced to $\boldsymbol{\Theta}^{(s)}_h = \{\rho_{T,h}, \phi_{T,h}, \rho_{R,h}, \phi_{R,h}\}$ and $\boldsymbol{\Theta}^{(c)}_h = \{x_{T,h}, y_{T,h}, x_{R,h}, y_{R,h}\}$, since we assume that $\theta_{T,h} = \theta_{R,h} = z_{T,h} = z_{R,h} = 0$, $\forall h \in \{1, ..., H\}$.

The example scenario of the system with ULAs in 2-D space is depicted in Figure 1, while an example scenario for the system in 3-D space with URAs is depicted in Figure 2.

In order to describe the signal model, we define the path differences between the reference transmit antenna and the m-th antenna in the transmit array in equation (1), and also between the reference receive antenna and the n-th antenna in the receive array in equation (2). The expressions in equations (1) and (2) are general and also apply to 2-D space if we assume that the z-coordinates are zero for all antennas and targets.

This definition of the path differences corresponds to the usage of the exact spherical wavefront model, which is adopted in this paper. By contrast, in case of the approximated wavefront model (the Fresnel approximation), the exact path differences are replaced by the second order Taylor approximations of (1) and (2), respectively.

In both 2-D and 3-D spaces, assuming the locations of transmit and receive arrays are known, two position estimates can be obtained for the each target (that may not always coincide). The distance between those two positions provides a measure for the reliability of these parameter estimates, as discussed later.

B. Signal model

The signal model of the 2-D and the 3-D estimation problems have the same structure. The signals obtained after matched filtering at the receiver for N pulses (snapshots) can be expressed using matrix notation as [4]

$$\boldsymbol{Y} = (\boldsymbol{A} \diamond \boldsymbol{B})\boldsymbol{D} + \boldsymbol{Z}, \tag{3}$$

where $\boldsymbol{Y} \in \mathbb{C}^{M_T M_R \times N}$ contains the received data after matched filtering (assuming unit transmit power), $\boldsymbol{Z}$ is the independently and identically distributed (i.i.d.) zero mean spatially and temporally white additive noise with variance σ^2, $\boldsymbol{D} \in \mathbb{C}^{H \times N}$ contains the complex reflection coefficients for each target in each snapshot. In the simulations they are modeled as zero mean i.i.d. random variables. Moreover, $\boldsymbol{A} = \begin{bmatrix} \boldsymbol{a}_1 & \boldsymbol{a}_2 & \dots & \boldsymbol{a}_H \end{bmatrix}$ represents the complex transmit array steering matrix, while $\boldsymbol{B} = \begin{bmatrix} \boldsymbol{b}_1 & \boldsymbol{b}_2 & \dots & \boldsymbol{b}_H \end{bmatrix}$ represents the complex receive array steering matrix. The elements of the array steering vectors for the h-th target are defined in terms of the path differences as follows

$$(\boldsymbol{a}_h)_{(m)} = e^{-j2\pi \frac{\delta^t_{m,h}}{\lambda}} \tag{4}$$

for the transmit steering vector, and

$$(\boldsymbol{b}_h)_{(n)} = e^{-j2\pi \frac{\delta^r_{n,h}}{\lambda}} \tag{5}$$

for the receive steering vector, where the notation $(\boldsymbol{x})_{(k)}$ denotes the k-th element of the vector $\boldsymbol{x}$. The exact expression of the array steering vectors $\boldsymbol{a}_h$ and $\boldsymbol{b}_h$ depends on the expressions of the path differences, which in turn are defined according to the adopted wavefront model, which could be exact (as in equations (1) and (2)), approximated by the Fresnel approximation [10], or approximated by the planar wavefront model if the sources are in the far-field.

In any of those cases, the data in (3) can be rearranged in the form of a 3-way array $\boldsymbol{\mathcal{Y}} \in \mathbb{C}^{M_T \times M_R \times N}$ such that its 3-mode unfolding is equal to

$$\boldsymbol{Y}^T = [\boldsymbol{\mathcal{Y}}]_{(3)} = \boldsymbol{D}^T (\boldsymbol{A} \diamond \boldsymbol{B})^T + [\boldsymbol{\mathcal{Z}}]_{(3)}, \tag{6}$$

where $\boldsymbol{\mathcal{Z}}$ contains the corresponding elements of $\boldsymbol{Z}^T$ and $\diamond$ denotes the Khatri-Rao (column-wise Kronecker) product.

This corresponds to the 3-mode unfolding of the noise corrupted CP decomposition of the tensor $\boldsymbol{\mathcal{Y}}$

$$\boldsymbol{\mathcal{Y}} = \boldsymbol{\mathcal{I}}_{3,H} \times_1 \boldsymbol{A} \times_2 \boldsymbol{B} \times_3 \boldsymbol{D}^T + \boldsymbol{\mathcal{Z}}, \tag{7}$$

where $\boldsymbol{\mathcal{I}}_{3,H}$ denotes the three-dimensional identity tensor of dimensions $H \times H \times H$.

This representation opens new ways to estimate the array steering matrices $\boldsymbol{A}$ and $\boldsymbol{B}$. Instead of using various decompositions of the sample covariance matrix $\boldsymbol{R} = \frac{1}{N}\boldsymbol{Y}\boldsymbol{Y}^H$, as suggested in [4], we resort to the direct application of an approximate CP decomposition to the received data. In particular, we apply the SECSI framework [14] to perform the approximate CP decomposition. Then, the final estimates are obtained via the solution of a system of linear equations. Note that the special case of this system of equations for the 2-D near-field localization with a ULA was already presented in [4].

III. Tensor-based Near-field localization

The TeNFiL algorithm consist of the four main stages - estimation of the steering matrices $\boldsymbol{A}$ and $\boldsymbol{B}$, phase unwrapping (estimation of the path differences), solution of the system of linear equations and parameter extraction. We describe each of them in the following.

ISBN 978-3-8007-4541-8

A. Estimation of the steering matrices

The first step of TeNFiL is to obtain estimates of the steering matrices $\boldsymbol{A}$ and $\boldsymbol{B}$. As already mentioned, the received data follows the noise corrupted low-rank representation in (7). Consequently, the estimates of the steering matrices can be obtained as loading matrices in an approximate CP decomposition of the tensor $\boldsymbol{\mathcal{Y}}$, which can be efficiently computed using the SECSI framework [14]. The estimates obtained in this step are denoted as $\hat{\boldsymbol{A}}$, $\hat{\boldsymbol{B}}$, and $\hat{\boldsymbol{D}}$. It should also be noted that this step is similar for both 2-D and 3-D estimation problems. For the simulations, we will use the "CON PS" heuristic of the SECSI framework [14].

Since the CP decomposition has a scaling ambiguity between the corresponding columns of $\hat{\boldsymbol{A}}$, $\hat{\boldsymbol{B}}$, and $\hat{\boldsymbol{D}}$, and since we know that $\delta^t_{T,1} = \delta_{R,1} = 0$, we can conclude that the first element of each column of $\boldsymbol{A}$ and $\boldsymbol{B}$ is equal to 1. To take this into account, we divide each column of $\hat{\boldsymbol{A}}$, $\hat{\boldsymbol{B}}$ by its first element, so that this constraint is satisfied.

A tensor-based model for near-field localization has already been briefly discussed in [16]. In contrast, the TeNFiL algorithm, which relies on the robust SECSI framework, provides a closed form solution to the estimation problem. Moreover, [16] relies on the ALS-based COMFAC algorithm proposed in [3], while the SECSI framework has an improved performance, especially for closely spaced targets. This is shown in [14] and [15], where COMFAC is compared to the SECSI solution. We also extend the TeNFiL algorithm to the estimation of the azimuth and elevation angles in a 3-D setting.

As already noted in [16], the CPD has an essential uniqueness of the resulting decomposition and also provides automatic pairing between the columns of $\hat{\boldsymbol{A}}$ and $\hat{\boldsymbol{B}}$. Thus, the estimated parameters are automatically paired.

B. Phase unwrapping

In order to get the proper estimates of the path differences, the phase unwrapping has to be applied to the principal angles of the elements of the steering vectors. The phase unwrapping problem is a topic of its own, but the problem at hand is somewhat simpler to the ones usually encountered in practice, mainly because of a much smaller dimensionality. For more details on the area, we refer the reader to [8].

Let us formally describe the unwrapping procedure. Let $\hat{\boldsymbol{a}}_h$ denote the h-th column of $\hat{\boldsymbol{A}}$ and $\hat{\boldsymbol{b}}_h$ denote the h-th column of $\hat{\boldsymbol{B}}$. Then, we express the unwrapping procedure via operator $\mathcal{U}\{\bullet\}$ as

$$\hat{\boldsymbol{\delta}}^t_h = \frac{\lambda}{2\pi} \cdot \mathcal{U}\{\angle \hat{\boldsymbol{a}}_h\}, \forall h \in \{1, ..., H\} \tag{8}$$

$$\hat{\boldsymbol{\delta}}^r_h = \frac{\lambda}{2\pi} \cdot \mathcal{U}\{\angle \hat{\boldsymbol{b}}_h\}, \forall h \in \{1, ..., H\} \tag{9}$$

where $\hat{\boldsymbol{\delta}}^t_h = \begin{bmatrix} \hat{\delta}^t_{1,h} & \hat{\delta}^t_{2,h} & \dots & \hat{\delta}^t_{M_T,h} \end{bmatrix}^T$ and $\hat{\boldsymbol{\delta}}^r_h = \begin{bmatrix} \hat{\delta}^r_{1,h} & \hat{\delta}^r_{2,h} & \dots & \hat{\delta}^r_{M_T,h} \end{bmatrix}^T$, and $\angle \boldsymbol{x}$ denotes the vector of principal angles of the complex vector $\boldsymbol{x}$.

TABLE I
PHASE UNWRAPPING IN THE SECOND STEP OF TENFIL

Usage scenario	Elements ordering	Unwrapping algorithm
ULA	From one end to another	1-d Itoh [11]
Arbitrary geometry	Ordering according to eq. (10)	
URA	Irrelevant	2-d Itoh [8]

The simplest and most commonly used algorithm for phase unwrapping is the Itoh's [11] algorithm for the unwrapping of one-dimensional signals. This is a simple algorithm that thresholds the consecutive jumps in phase between adjacent samples to be less than π, and detects a phase wrap if this condition is false. When the phase wrap is detected, all consequent samples are shifted by $\pm 2\pi$. The original phase can be properly recovered, assuming that the noise is not too high and the signal is not aliased.

This approach is appropriate in case of a ULA, since the elements of $\boldsymbol{a}_h$ can be considered as samples of a one-dimensional function with uniform sampling intervals. For more general cases of arbitrary array geometries, we also resort to this method, although it is heuristic. The only difference is that care should be taken regarding the ordering of the antennas, since the algorithm can fail if consecutive antennas will be relatively far away from each other (this can lead to a false phase wrap). To apply the Itoh algorithm to general antenna geometries, we define the ordering in such a way that each next antenna index is assigned to the antenna with the smallest Euclidean distance among those that are left. More formally, we can express it as (we drop transmit and receive superscripts for brevity)

$$\ell_{m,m+1} < \ell_{m,i}, \forall i \in \{m+2, ..., M\}, \, m \in \{1, ..., M\} \tag{10}$$

where $\ell_{m,k} = \sqrt{(x_m - x_k)^2 + (y_m - y_k)^2 + (z_m - z_k)^2}$, and x_m, y_m, z_m (x_k, y_k, z_k) denote the Cartesian coordinates of the m-th (k-th) antenna in the array (assume $z_m = z_k = 0$ for two-dimensional space). Since it is commonly assumed that the spacing between antennas does not exceeds $\lambda/2$, then such an antenna numbering will guarantee that the signal is not aliased.

In case of URAs there is a better way to perform phase unwrapping. Since a URA corresponds to sampling in 2-D space with a uniform two-dimensional grid, the two-dimensional extension of Itoh's algorithm can be applied [8]. In this case, the ordering is irrelevant. We summarize the phase unwrapping step of TeNFiL in Table I.

C. Solution of the system of linear equations

This step is independently applied for each column of $\hat{\boldsymbol{A}}$ and $\hat{\boldsymbol{B}}$. For notational simplicity, we drop the transmit and receive subscripts (T and R), since we use the same processing for the transmit and the receive steering vectors. The coordinates with subscripts m denote the coordinates of the antennas (transmit or receive), while the coordinates with subscripts h denote estimated coordinates of the targets with respect to the local

ISBN 978-3-8007-4541-8

TABLE II
SYSTEMS OF EQUATIONS FOR THE THIRD STEP OF TENFIL

Scenario	Arbitrary geometry	Special case (ULA or URA)
2-*D space*	$2\underbrace{\begin{bmatrix} x_2 & y_2 & \hat{\delta}_{2,h} \\ x_3 & y_3 & \hat{\delta}_{3,h} \\ \vdots & \vdots & \vdots \\ x_M & y_M & \hat{\delta}_{M,h} \end{bmatrix}}_{\boldsymbol{X}_h \in \mathbb{R}^{M-1\times 3}} \boldsymbol{w}_h = \underbrace{\begin{bmatrix} d_2^2 - \hat{\delta}_{2,h}^2 \\ d_3^2 - \hat{\delta}_{3,h}^2 \\ d_4^2 - \hat{\delta}_{4,h}^2 \\ \vdots \\ d_M^2 - \hat{\delta}_{M,h}^2 \end{bmatrix}}_{\boldsymbol{Y}_h \in \mathbb{R}^{M-1\times 1}}$ (11) where $\boldsymbol{w}_h = \begin{bmatrix} x_h \\ y_h \\ \sqrt{x_h^2 + y_h^2} \end{bmatrix} = \begin{bmatrix} \rho_h \cos(\phi_h) \\ \rho_h \sin(\phi_h) \\ \rho_h \end{bmatrix}$ (12)	ULA: $2\underbrace{\begin{bmatrix} x_2 & \hat{\delta}_{2,h} \\ x_3 & \hat{\delta}_{3,h} \\ \vdots & \vdots \\ x_M & \hat{\delta}_{M,h} \end{bmatrix}}_{\boldsymbol{X}_h \in \mathbb{R}^{M-1\times 2}} \boldsymbol{w}_h = \underbrace{\begin{bmatrix} d_2^2 - \hat{\delta}_{2,h}^2 \\ d_3^2 - \hat{\delta}_{3,h}^2 \\ d_4^2 - \hat{\delta}_{4,h}^2 \\ \vdots \\ d_M^2 - \hat{\delta}_{M,h}^2 \end{bmatrix}}_{\boldsymbol{Y}_h \in \mathbb{R}^{M-1\times 1}}$ (13) where $\boldsymbol{w}_h = \begin{bmatrix} x_h \\ \sqrt{x_h^2 + y_h^2} \end{bmatrix} = \begin{bmatrix} \rho_h \cos(\phi_h) \\ \rho_h \end{bmatrix}$ (14)
3-*D space*	$2\underbrace{\begin{bmatrix} x_2 & y_2 & z_2 & \hat{\delta}_{2,h} \\ x_3 & y_3 & z_3 & \hat{\delta}_{3,h} \\ \vdots & \vdots & \vdots & \vdots \\ x_M & y_M & z_M & \hat{\delta}_{M,h} \end{bmatrix}}_{\boldsymbol{X}_h \in \mathbb{R}^{M-1\times 4}} \boldsymbol{w}_h = \underbrace{\begin{bmatrix} d_2^2 - \hat{\delta}_{2,h}^2 \\ d_3^2 - \hat{\delta}_{3,h}^2 \\ \vdots \\ d_M^2 - \hat{\delta}_{M,h}^2 \end{bmatrix}}_{\boldsymbol{Y}_h \in \mathbb{R}^{M-1\times 1}}$ (15) where $\boldsymbol{w}_h = \begin{bmatrix} x_h \\ y_h \\ z_h \\ \sqrt{x_h^2 + y_h^2 + z_h^2} \end{bmatrix} = \begin{bmatrix} \rho_h \cos(\phi_h)\cos(\theta_h) \\ \rho_h \sin(\phi_h)\cos(\theta_h) \\ \rho_h \sin(\theta_h) \\ \rho_h \end{bmatrix}$ (16)	URA: $2\underbrace{\begin{bmatrix} x_2 & y_2 & \hat{\delta}_{2,h} \\ x_3 & y_3 & \hat{\delta}_{3,h} \\ \vdots & \vdots & \vdots \\ x_M & y_M & \hat{\delta}_{M,h} \end{bmatrix}}_{\boldsymbol{X}_h \in \mathbb{R}^{M-1\times 3}} \boldsymbol{w}_h = \underbrace{\begin{bmatrix} d_2^2 - \hat{\delta}_{2,h}^2 \\ d_3^2 - \hat{\delta}_{3,h}^2 \\ \vdots \\ d_M^2 - \hat{\delta}_{M,h}^2 \end{bmatrix}}_{\boldsymbol{Y}_h \in \mathbb{R}^{M-1\times 1}}$ (17) where $\boldsymbol{w}_h = \begin{bmatrix} x_h \\ y_h \\ \sqrt{x_h^2 + y_h^2 + z_h^2} \end{bmatrix} = \begin{bmatrix} \rho_h \cos(\phi_h)\cos(\theta_h) \\ \rho_h \sin(\phi_h)\cos(\theta_h) \\ \rho_h \end{bmatrix}$ (18)

system of coordinates. Taking the estimates obtained in (8) or (9), squaring and rearranging (1) or (2) we get

$$\hat{\delta}_{m,h}^2 + 2\hat{\delta}_{m,h}\rho_h = d_m^2 - 2(x_m x_h + y_m y_h + z_m z_h) \quad (19)$$

where $d_m^2 = x_m^2 + y_m^2 + z_m^2$, $h \in \{1, ..., H\}$, $m \in \{2, ..., M\}$, and $M \in \{M_T, M_R\}$.

Rearranging this equation results in

$$2x_m x_h + 2y_m y_h + 2z_m z_h + 2\hat{\delta}_{m,h}\rho_h = d_m^2 - \hat{\delta}_{m,h}^2 \quad (20)$$

which can be interpreted as a set of $M-1$ linear equations (since $\hat{\delta}_{1,h} = 0\ \forall h$) with respect to four unknowns x_h, y_h, z_h, and $\rho_h = \sqrt{x_h^2 + y_h^2 + z_h^2}$.

Based on that most general expression, we can easily derive similar systems for more special cases, such as 3-D estimation with a URA or 2-D estimation with a ULA. We summarize the resulting respective systems in Table II. In all cases, the vector $\boldsymbol{w}_h$ denotes the solution vector for the system of equations for the h-th target.

The described set of equations in (15) is the most general. It allows to estimate the location of the targets in the full 3-D space, provided that the antenna array geometry exhibits diversity in all spatial directions. If this is not the case, the matrix $\boldsymbol{X}_h$ will not have full column rank, which is the case if we use, for example, a URA. In such a situation, we choose a local system of coordinates with the origin at the reference antenna such that all antennas lie in the x-y-plane. In that case, $z_m = 0\ \forall m$. Then, the system in (15) and solution vector in (16) reduce to (17) and (18), respectively. In that case we can only estimate the locations of the target in that half of the 3-D space where $z_h > 0$ (or $0 \leq \theta_h \leq \pi/2$), as can be observed from (18).

Next, consider estimation in 2-D space. In that case, $z_m = z_h = 0$ and $\cos(\theta_h) = 1\ \forall m, h$. Then, the system in (15) and solution vector in (16) reduce to (11) and (12), respectively. In this case, it is possible to estimate the locations of the targets in the full 2-D space, provided that the array has a diversity in two orthogonal directions. Otherwise, for example, in case of a ULA, the columns of $\boldsymbol{X}_h$ will be linearly dependent. In that case, we choose a local system of coordinates such that all antennas lie on the x-axis, i.e., $y_m = 0\ \forall m$. Then, the system in (11) and the solution vector in (12) reduce to (13) and (14), respectively.

The solution vector can be found by means of the LS or the Total Least Squares (TLS) solution. In the latter case, the solution vector $\boldsymbol{w}_h$ is found as

$$\boldsymbol{w}_h = (\boldsymbol{v}_h)_{(1:q-1)} / (\boldsymbol{v}_h)_{(q)} \quad (21)$$

where q is the number of elements in $\boldsymbol{w}_h$, and $\boldsymbol{v}_h$ is the right-singular vector of the augmented matrix $\begin{bmatrix} \boldsymbol{X}_h & \boldsymbol{Y}_h \end{bmatrix}$ that corresponds to the smallest singular value [4], [9]. However,

ISBN 978-3-8007-4541-8

the LS solution (used in the simulations) shows the same performance as the TLS solution.

D. Parameter extraction

In the last step of TeNFiL, we compute the parameters of each target based on $\boldsymbol{w}_h$. In case of the general 3-D space configuration in (16), the parameters are

$$\rho_h = (\boldsymbol{w}_h)_{(4)} \tag{22a}$$

$$\phi_h = \text{atan2}\left(\frac{(\boldsymbol{w}_h)_{(2)}}{\rho_h}, \frac{(\boldsymbol{w}_h)_{(1)}}{\rho_h}\right) \tag{22b}$$

$$\theta_h = \text{atan2}\left(\frac{(\boldsymbol{w}_h)_{(3)}}{\rho_h}, \frac{\sqrt{(\boldsymbol{w}_h)_{(1)}^2 + (\boldsymbol{w}_h)_{(2)}^2}}{\rho_h}\right) \tag{22c}$$

where $\text{atan2}(y, x)$ denotes the four quadrant arctangent function. In case of a URA, the distance is equal to $\rho_h = (\boldsymbol{w}_h)_{(3)}$ and the elevation is computed as

$$\theta_h = \cos^{-1}\left(\frac{\sqrt{(\boldsymbol{w}_h)_{(1)}^2 + (\boldsymbol{w}_h)_{(2)}^2}}{\rho_h}\right) \tag{23}$$

The only difference for general 2-D estimation in (12) is that $\rho_h = (\boldsymbol{w}_h)_{(3)}$ and we do not estimate the elevation. For a ULA in 2-D space we define the azimuth as

$$\phi_h = \cos^{-1}\left(\frac{(\boldsymbol{w}_h)_{(1)}}{\rho_h}\right) \tag{24}$$

The equations (23) and (24) show that a simple reliability test can be applied in those cases. If the value of $(\boldsymbol{w}_h)_{(1)}/\rho_h$ or $\sqrt{(\boldsymbol{w}_h)_{(1)}^2 + (\boldsymbol{w}_h)_{(2)}^2}/\rho_h$ is larger than one, then the test has failed and the parameter estimates are not reliable.

Moreover, since the algorithm provides two estimates of the locations of the targets, we can derive a reliability measure as the Euclidean distance between the two estimates as

$$\Delta_h = \sqrt{(\hat{x}_{T,h} - \hat{x}'_{R,h})^2 + (\hat{y}_{T,h} - \hat{y}'_{R,h})^2 + (\hat{z}_{T,h} - \hat{z}'_{R,h})^2} \tag{25}$$

where $\hat{x}'_{R,h} = \hat{x}_{R,h} + x_R$, $\hat{y}'_{R,h} = \hat{y}_{R,h} + y_R$ and $\hat{z}'_{R,h} = \hat{z}_{R,h} + z_R$, and x_R, y_R and z_R are receive array reference antenna coordinates. It is assumed here that the local transmit and receive systems of coordinates are not rotated with respect to each other, otherwise the estimated parameters should first be rotated accordingly.

IV. Simulation Results

For the simulations we use a URA with $M_{T,x} = M_{R,x} = 5$ antennas along the x-axes and $M_{T,y} = M_{R,y} = 5$ antennas along the y-axes, which totally results in $M_T = M_R = 25$ antennas in the transmit and the receive arrays. The reference receive antenna is located at $x_R = 4\lambda$, $y_R = z_R = 0$, i.e., both antenna arrays are located in the x-y-plane, as depicted in Figure 2. The number of snapshots is set to $N = 20$. The inter-element spacing for the URA is set to $d_T = d_R = \lambda/2$, where $\lambda = 1.5$ cm. However, all the distances and errors in the following are normalized with respect to λ. The resulting measurement tensor is of size $25 \times 25 \times 20$.

The parameters of the $H = 3$ targets are chosen to be equal to $\boldsymbol{\Theta}_1 = \{4.9\lambda, 33.7°, 45°, 4.1\lambda, 120.3°, 57.3°\}$, $\boldsymbol{\Theta}_2 = \{5.1\lambda, 33.7°, 45°, 4.2\lambda, 116.6°, 58.2°\}$, and $\boldsymbol{\Theta}_3 = \{5\lambda, 31.6°, 43.4°, 4.06\lambda, 114.6°, 58.6°\}$. This simulation scenario corresponds to three targets located in the plane that passes through the x-axis under $45°$ angle with respect to the x-y-plane. The second target has the same distance to the closest transmit and receive antennas, and the locations of the first and the third targets are obtained via slightly shifting the location of the second target towards the transmit and the receive array, respectively. Such a choice of the target locations results in similar condition numbers for transmit and receive steering matrices, which is $\text{cond}(\boldsymbol{A}) = \text{cond}(\boldsymbol{B}) \approx 111$ and corresponds to a challenging scenario for the algorithms that compute an approximate CP decomposition.

In the first simulation, we change the SNR, which is defined as $1/\sigma^2$. We compute the root mean square error (RMSE) for different parameters that are to be estimated as follows

$$\text{RMSE} = \sqrt{\frac{1}{T}\sum_{k=1}^{K}\sum_{h=1}^{H} \text{I}_{k,h} \cdot (e_{k,h})^2}, \tag{26}$$

$$e_{k,h} = a_h - \hat{a}_{k,h}, \quad T = \sum_{k=1}^{K}\sum_{h=1}^{H} \text{I}_{k,h} \tag{27}$$

where $a_h \in \{\rho_{T,h}, \phi_{T,h}, \theta_{T,h}, \rho_{R,h}, \phi_{R,h}, \theta_{R,h}\}$ and $\hat{a}_{k,h}$ is an estimate of a_h in the k-th trial. The quantity $\text{I}_{k,h}$ denotes the indicator that the reliability test described in Subsection III-D has been passed, i.e., $\text{I}_{k,h} = \text{I}\{\sqrt{(\boldsymbol{w}_{k,h})_{(1)}^2 + (\boldsymbol{w}_{k,h})_{(2)}^2}/\rho_{k,h} < 1\}$, where $\text{I}\{A\}$ denotes the indicator function that is equal to 1 when the condition A is satisfied, and 0 otherwise. Moreover, T denotes the total number of cases where the reliability test has not failed.

In addition to the separate RMSE in each parameter, we also define the RMSE in terms of the Euclidean distance between the estimated and the true locations of the targets. We define the errors in this case as $e_{k,h} = ||\boldsymbol{c}_h - \hat{\boldsymbol{c}}_{k,h}||$, where $\boldsymbol{c}_h$ denotes

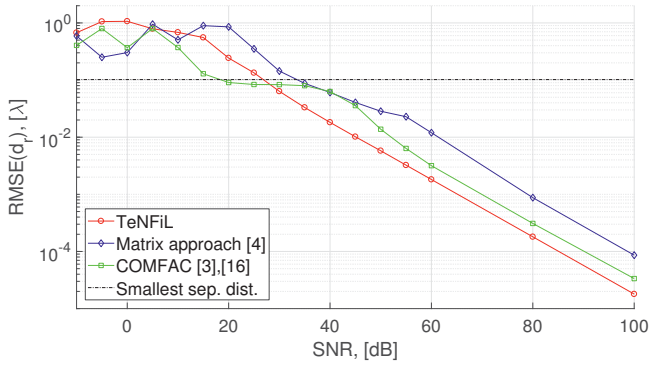

Fig. 3. RMSE in Euclidean distance on transmit side vs. SNR. The results were averaged over $K = 10000$ trials. The TeNFiL algorithm outperforms the 3-D extension of the matrix approach used in [4] and the COMFAC [3] algorithm to estimate the steering matrices. The dash-dotted line represents half of the smallest distance between all the targets in the scenario.

ISBN 978-3-8007-4541-8

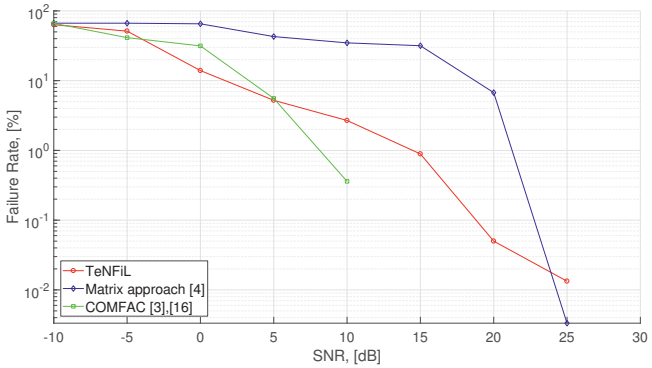

Fig. 4. Reliability test failure rate vs. SNR. The number of reliability test failures drops as the SNR increases.

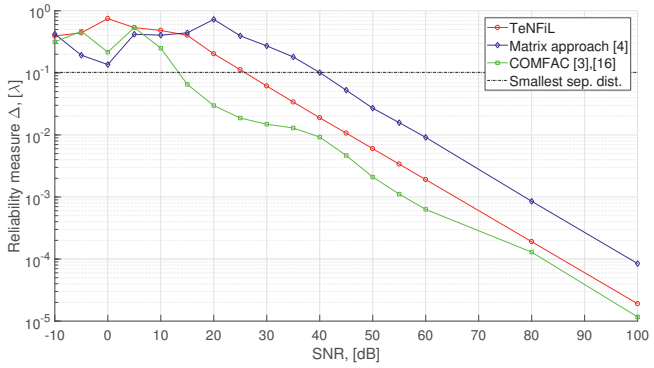

Fig. 6. Reliability measure (average separation distance) vs. SNR, defined in equation (25). The separation distance reduces as the SNR increases. The dash-dotted line represents half of the smallest distance between all the targets in the scenario.

the vector of Cartesian coordinates of the h-th target (defined with respect to to the transmit or the receive side), and $\hat{\boldsymbol{c}}_{k,h}$ is its estimate in the k-th trial.

The simulation results are depicted in Figure 3. We depict only errors obtained at the transmit side for brevity, the results obtained on the receive side are similar due to the symmetry of the chosen scenario. We compare the performance of the proposed TeNFiL algorithm with other approaches for the estimation of the steering matrices $\boldsymbol{A}$ and $\boldsymbol{B}$ (all other steps are similar to those in TeNFiL algorithm). The blue curve shows the performance of the estimation algorithm proposed in [4], while the green curve corresponds to the use of the ALS-based approximate CP decomposition algorithm COMFAC [3], also applied in [16]. The black dash-dotted line denotes the half of the smallest Euclidean distance between the targets. The error below that line indicates that all three targets are properly resolved.

From the Figure 3 we observe that TeNFiL outperforms all considered alternatives, especially the matrix approach from [4]. We can also observe that in such challenging scenario the targets are only properly resolved for high SNRs ($>$ 30 dB). Note that the curves are less smooth at low SNRs due to the high number of reliability test failures, which can be observed in Figure 4, where we depict the reliability test failure rate, defined as $100 \cdot T/KH$ [%]. The higher number of reliability test failures reduces the available number of samples to average the errors and the curves become noisy.

In Figure 5 we depict the averaged execution time for each algorithm. For the simulations we use the "CON PS" [14] heuristic that is one of the computationally most efficient heuristics of the SECSI framework. From the figure we can observe that TeNFiL is significantly faster than the other algorithms, especially the COMFAC algorithm. The execution time of COMFAC is not stable because of its iterative nature and varies depending on the SNR.

The averaged separation distance between estimates obtained on the transmit side and the receive side (reliability measure in equation (25)) is depicted in Figure 6. It can be observed that the reliability measure decreases with the SNR. Around 30 dB SNR it becomes smaller than the half of the smallest Euclidean distance between the targets. Consequently, this reliability measure allows to assess the consistency of the obtained estimates and can serve as an estimate of the SNR.

In the second simulation, we visualize the performance of

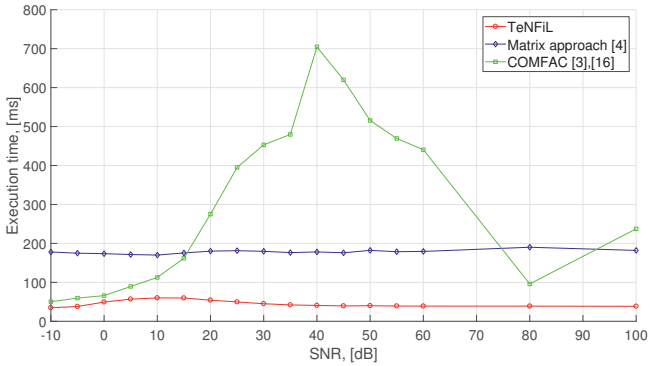

Fig. 5. Average execution time vs. SNR. The TeNFiL algorithm requires much less computational time then the other algorithms due to the reduced complexity of the underlying SECSI framework.

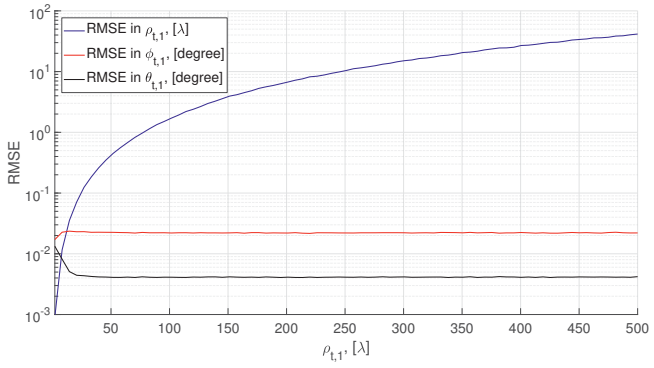

Fig. 7. RMSE for distance, azimuth and elevation estimated on the transmit side vs. the distance to the transmit array reference antenna $\rho_{t,1}$. The error in elevation and azimuth does not depend on the distance, while the error in distance increases with $\rho_{t,1}$.

ISBN 978-3-8007-4541-8

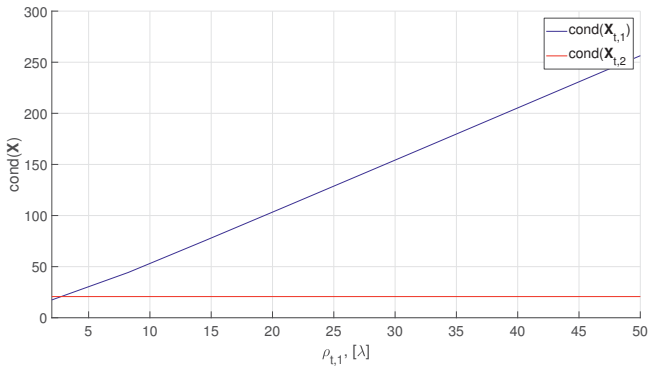

Fig. 8. The averaged condition number of the matrix $\boldsymbol{X}_h$ vs. the z_1 coordinate of the target. The condition number on both transmit and receive sides increases as we move away from the array.

the TeNFiL algorithm in the far-field region. In order to do that, we consider a scenario with two targets. We set the initial parameters of the targets with respect to transmit array to $\rho_{t,1} = 2\lambda$, $\phi_{t,1} = 45°$, $\theta_{t,1} = 45°$ and $\rho_{t,2} = 4\lambda$, $\phi_{t,2} = -45°$, $\theta_{t,2} = 45°$, respectively. The SNR is fixed to 30 dB. Next, we vary the distance of the first target to transmit array $\rho_{t,1}$ from 2λ to 500λ, in order to see the performance as the target moves away from the arrays. The number of trials is 2000 in this simulation, and the RMSEs of the parameters are depicted in Figure 7.

From the results it can be observed that the error for elevation and azimuth estimation does not depend on the distance, while the error in distance increase as we move away from the array, which is expected since in the far-field region the wavefront is planar and does not provide any information about the distance to the source. The increase in error can be explained by the fact that in the far-field the path differences (or delays) will form a linear combination of the antenna coordinates, and thus the $\boldsymbol{X}_{t,1}$ in both (15) and (17) will not have full column rank. We can observe this effect by the condition number of $\boldsymbol{X}_{t,1}$, see Figure 8, which increases as we move away from the antenna array, while the condition number of $\boldsymbol{X}_{t,2}$ stays constant since the second target stays in the near-field region.

V. Conclusions

In this paper the high-resolution tensor-based near-field localization algorithm for Bistatic MIMO Radar system TeNFiL is proposed. The proposed algorithm performs the parameter estimation of the dominant radar targets in 3-D space based on the exact wavefront model and is applicable to arbitrary array geometries. Moreover, the algorithm is able to additionally provide a reliability test, if we restrict the estimation to only half of the full 3-D space. It can also provide a soft reliability measure that helps to assess the consistency of the obtained estimates. The simulation results show that the SECSI framework, which is chosen to estimate the steering matrices in the TeNFiL algorithm, provides better performance than the ALS based COMFAC algorithm in critical scenario. Moreover, it has a significantly lower computational complexity. In the simulations we also analyze the performance of the algorithm as we get closer to the far-field region. As the target moves away from the antenna arrays, the estimation error for distance grows, while for the elevation and the azimuth its stays constant. The condition number of the resulting system of equations provides a simple measure of reliability of the distance estimate and can potentially be used to separate near-field and far-field sources in the framework of one estimation algorithm.

References

[1] T. Bao, M. N. El Korso, and H. H. Ouslimani, "Cramér–Rao bound and statistical resolution limit investigation for near-field source localization", *Digital Signal Processing*, vol. 48, pp. 137–147, 2016.

[2] Y. Begriche, M. Thameri, and K. Abed-Meraim, "Exact Cramer Rao bound for near field source localization", in *Proc. 11th Int. Conf. Information Science, Signal Processing and their Applications (ISSPA)*, pp. 718–721, July 2012.

[3] R. Bro, N. D. Sidiropoulos, and G. B. Giannakis, "A fast least squares algorithm for separating trilinear mixtures", in *Proc. of Int. Workshop Independent Component Analysis and Blind Signal Separation*, pp. 11–15, 1999.

[4] P. Chargé, Y. Wang, and P. R. Singh, "Near field targets localization using bistatic MIMO system with spherical wavefront based model", in *Proc. 25th European Signal Processing Conf. (EUSIPCO)*, pp. 2408–2412, Aug. 2017.

[5] L. de Lathauwer, B. de Moor, and J. Vanderwalle, "A multilinear singular value decomposition", *SIAM J. Matrix Anal. Appl.*, vol. 21, no. 4, 2000.

[6] E. Fishler, A. Haimovich, R. Blum, D. Chizhik, L. Cimini, and R. Valenzuela, "MIMO radar: an idea whose time has come", in *Proc. IEEE Radar Conf. (IEEE Cat. No.04CH37509)*, pp. 71–78, Apr. 2004.

[7] H. Gazzah and J. P. Delmas, "CRB-Based Design of Linear Antenna Arrays for Near-Field Source Localization", *IEEE Transactions on Antennas and Propagation*, vol. 62, no. 4, pp. 1965–1974, Apr. 2014.

[8] D. C. Ghiglia and M. D. Pritt, *Two-Dimensional Phase Unwrapping: Theory, Algorithms, and Software*, vol. 4, Wiley New York, 1998.

[9] Gene H Golub and Charles F Van Loan, *Matrix computations*, vol. 3, JHU Press, 2012.

[10] M. Haardt, R. N. Challa, and S. Shamsunder, "Improved bearing and range estimation via high-order subspace based Unitary ESPRIT", in *Proc. 30th Asilomar Conf. Signals, Systems and Computers*, vol. 1, pp. 380–384 vol.1, Nov. 1996.

[11] K. Itoh, "Analysis of the phase unwrapping problem", *Applied Optics*, vol. 21, no. 14, pp. 2470, July 1982.

[12] M. N. E. Korso, R. Boyer, A. Renaux, and S. Marcos, "Conditional and unconditional Cramér–Rao bounds for near-field source localization", *IEEE Transactions on Signal Processing*, vol. 58, no. 5, pp. 2901–2907, May 2010.

[13] J. Li and P. Stoica, *MIMO Radar Signal Processing*, John Wiley, 2009.

[14] F. Roemer and M. Haardt, "A semi-algebraic framework for approximate CP decompositions via Simultaneous Matrix Diagonalizations (SECSI)", *Elsevier Signal Processing*, vol. 93, no. 9, pp. 2722–2738, 2013.

[15] F. Roemer, C. Schroeter, and M. Haardt, "A semi-algebraic framework for approximate CP decompositions via joint matrix diagonalization and generalized unfoldings", in *Proc. of the 46th Asilomar Conf. Signals, Systems, and Computers*, pp. 2023–2027, Nov. 2012.

[16] P. R. Singh, Y. Wang, and P. Chargé, "Bistatic MIMO radar for near field source localisation using PARAFAC", *Electronics Letters*, vol. 52, no. 12, pp. 1060–1061, 2016.

[17] P. R. Singh, Y. Wang, and P. Chargé, "Near field targets localization using bistatic MIMO system with symmetric arrays", in *Proc. 25th European Signal Processing Conf. (EUSIPCO)*, pp. 2403–2407, Aug. 2017.

[18] E. Zhou, H. Jiang, and H. Qi, "4-D parameter estimation in bistatic MIMO radar for near-field target localization", in *Proc. IEEE Int. Wireless Symp. (IWS 2015)*, pp. 1–4, Mar. 2015.

